



# Understanding the Formation of Strain-Induced Martensite in Hydrogen Charged Austenitic Stainless Steel using Nanoprobe STEM

Julian E.C. Sabisch, Christopher W. San Marchi, Joseph A. Ronevich, Douglas L. Medlin

## Interest on Hydrogen Effects in Steel

Stainless steels (SS) are used in a wide variety of structural applications involving reactive environments. The presence of hydrogen can negatively affect the mechanical properties of stainless steels, resulting in strain localization leading to embrittlement and fracture. What effects hydrogen has on the microstructure of one of the most common stainless steels (304L) is of great interest when engineering low cost systems in highly reactive environments.

For this experiment, a forged sample of 304L SS (Figure 1) was strained after charging to 140wppm hydrogen content and without hydrogen charging. Characteristic flow stress curves tested to fracture show (right) a large effect on both ductility and strength due to hydrogen-charging (HC)

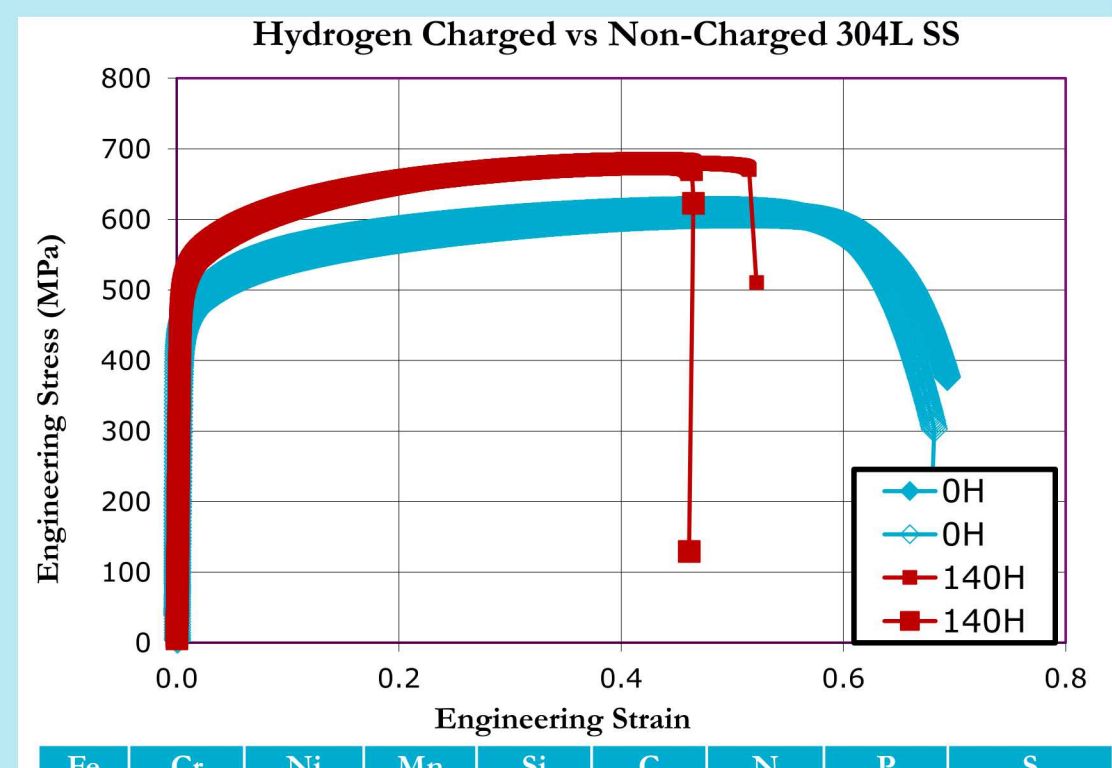


Figure 1: Composition and mechanical data for 304L SS samples tested to fracture. Hydrogen charging has a large effect on macroscopic response.

## Nanobeam Diffraction Characterization

Small angle (0.21 mrad) convergent beam nanodiffraction was used to probe the microstructure for both loading conditions. Nanobeam diffraction allows for site specific probing of crystal structure.

- A spatial resolution (beam diameter) of  $\sim 3$ nm was achieved in diffraction analysis, probing local microstructural changes within shear bands.
- Twinning and secondary phases can be pinpointed to specific areas within the microstructure.
- The streaking observed in diffraction patterns allows the characterization of the habit planes of platelets; here streaking along  $\{111\}$  reflections is due to  $\epsilon$ -martensite and twin platelets forming from stacking faults ( $\frac{a}{6}\langle 112 \rangle$  partial dislocations) on  $\{111\}$  planes.

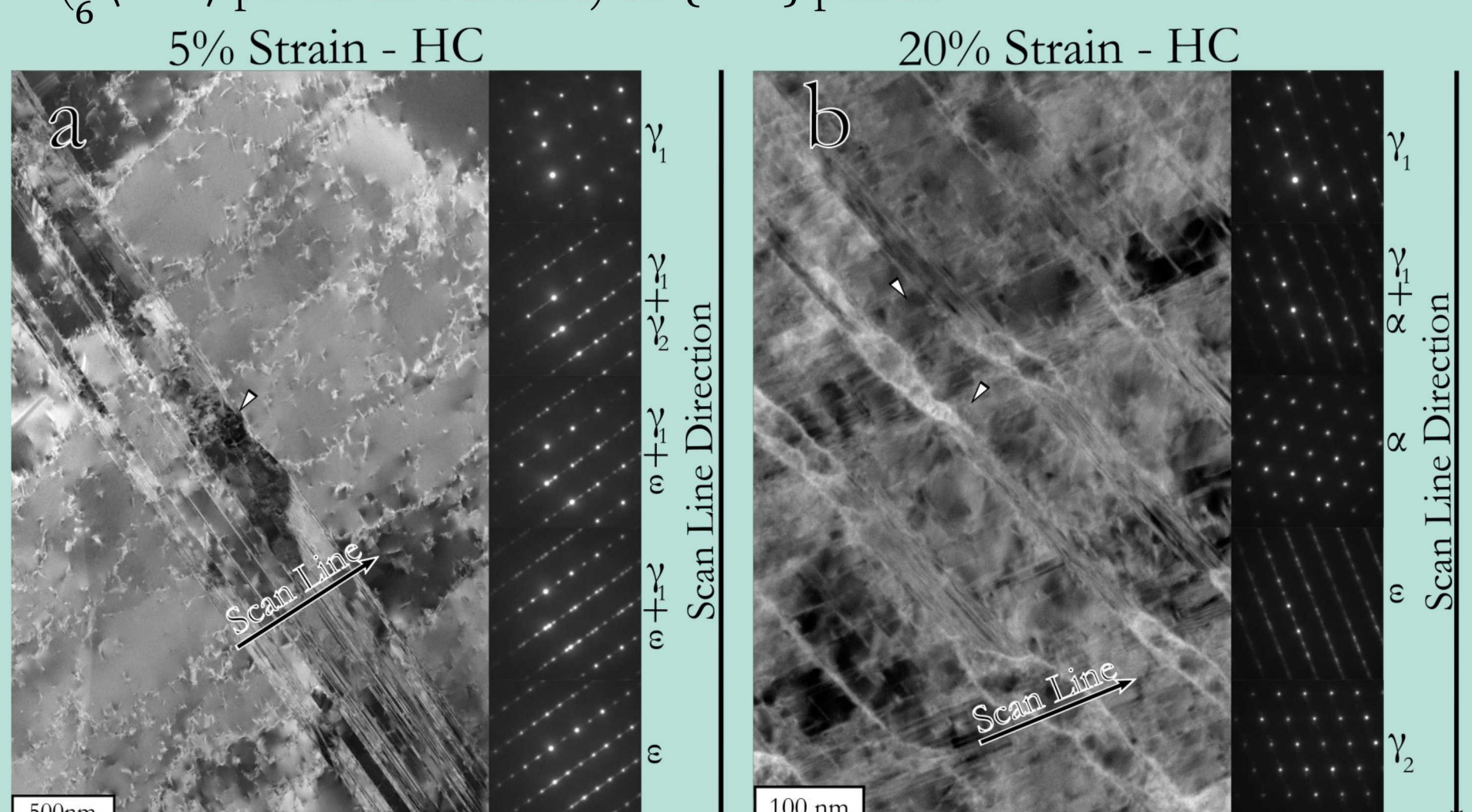


Figure 3: DC-STEM image of 5% strain HC sample and the 20% strain HC sample. Triangles mark slip bands in the microstructure within which martensite platelets have formed. At 5% strain only one shear band is observed, containing both twins and  $\epsilon$ -martensite platelets. At 20% strain double shearing has occurred, with shear bands intersecting to form  $\alpha$ -martensite from two shear bands containing  $\gamma$ -twins and  $\epsilon$ -martensite. This is consistent with the classic Olson-Cohen double shear mechanism.

## HR-STEM of Martensite Nucleus

HR-STEM was performed to observe the interfacial structure of  $\alpha$ -martensite nucleus within a 20% strain HC-SS  $\epsilon$ -martensite shear band.

- Interfaces between  $\gamma$ -austenite and  $\epsilon$ -martensite is largely coherent and strain free, showing  $\bar{b} = \frac{1}{2}\langle 1011 \rangle_{\epsilon}$  dislocations populating the  $\gamma/\epsilon$  boundary.
- Stepped interfaces between  $\gamma$  and  $\epsilon$  phases are consistent with the Burgers' vector of  $\bar{b} = \frac{a}{4}\langle 12\bar{1} \rangle_{\gamma}$  dislocation, however the step is continuous forming  $\alpha$ -like region, as first proposed by Burger and Bogers.
- The intersection of two  $\epsilon$ -martensite laths appear to be required to form  $\alpha$ -martensite as seen in the Olson-Cohen mechanism<sup>[4]</sup>.
- Morphologies of  $\alpha$ -martensite regions show that the formation of  $\alpha$ -martensite is entirely contained within  $\epsilon$ -martensite laths, expanding to grow along the shear band.

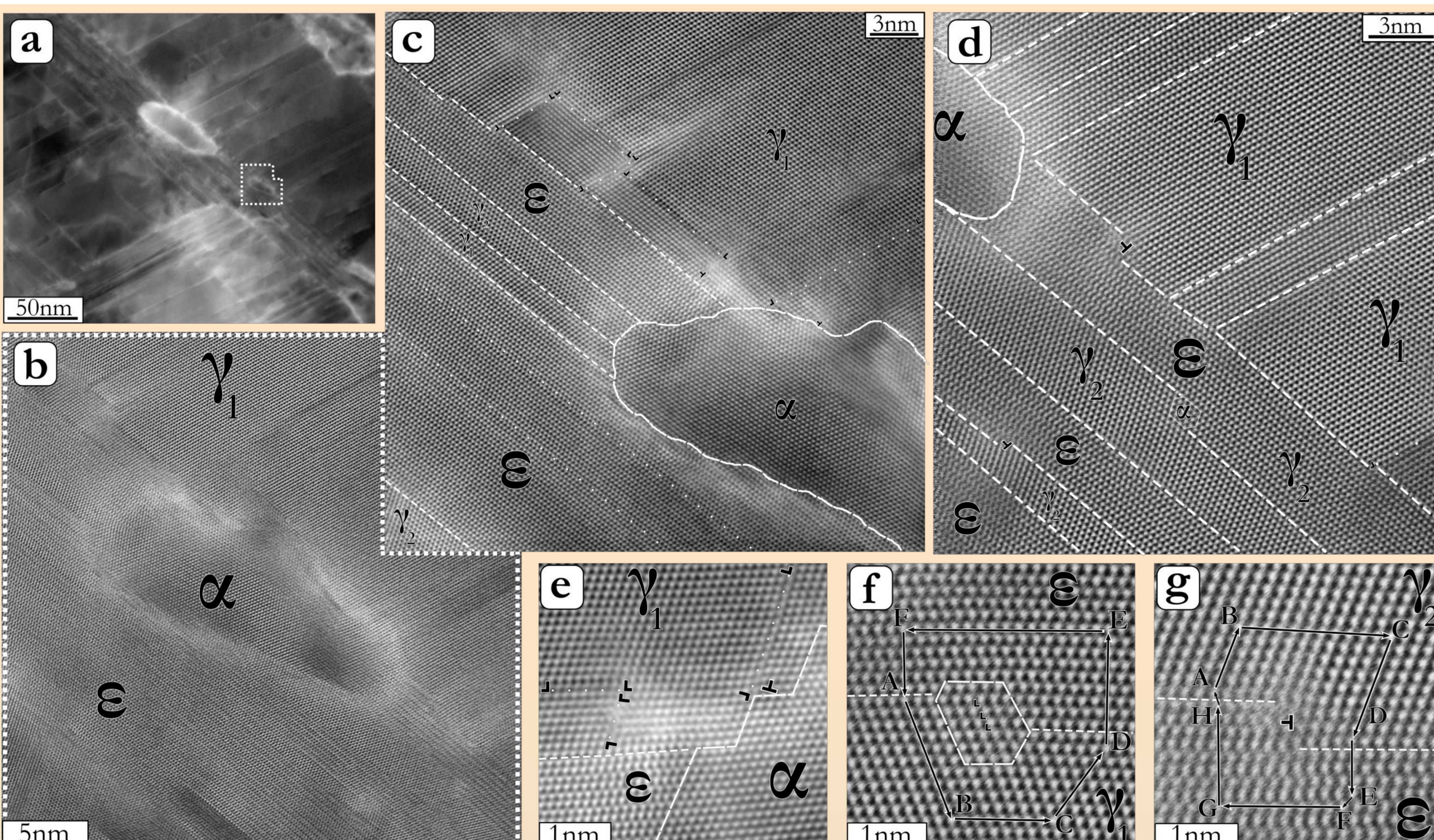


Figure 6: Overview of area where HR-STEM images were taken a) from a similar area as seen in Figure 3b). HR-STEM overview image b) of  $\alpha$ -martensite nuclei formed at the intersection of two  $\epsilon$ -martensite containing shear. HR-STEM image of top c) and bottom d) of  $\alpha$ -martensite nucleus with phases, twins, phase boundaries, dislocations, and stacking faults marked. e-g) show zoom inserts of atomic positions at phase boundaries containing dislocations. f) shows a  $\bar{b} = \frac{a}{4}\langle 110 \rangle_{\gamma} + \frac{a}{4}\langle 12\bar{1} \rangle_{\gamma}$  dislocation creating a region containing  $\alpha$ -like atomic spacings along the stepped  $\gamma/\epsilon$  interface. g) interfacial  $\bar{b} = \frac{1}{2}\langle 1011 \rangle_{\epsilon}$  dislocation.

## Experiment and Technique Overview

Samples unloaded after 5% and 20% strain for both HC and non-charged (NC) conditions were sectioned and electro-polished for observation in a Thermo Fisher Scientific FEI Themis Z probe corrected scanning transmission electron microscope (STEM).

- Diffraction contrast STEM (DC-STEM) was used for large scale microstructure observations as it allows for imaging both planar defects, secondary phase objects, and dislocations with great detail.<sup>[1]</sup>
- DC-STEM allows for quick convergence angle changes to investigate the crystal structure through nanodiffraction ( $\alpha = 0.21$  mrad), which provides diffraction patterns similar to conventional TEM selected area diffraction.
- High-resolution (HR) high angle ( $\alpha = 21.4$  mrad) annular dark field (HAADF) STEM was used for atomic resolution scans observing the interfaces between phases and the varied dislocations dislocation character of the interface.
- HR-STEM imaging is extremely sensitive to crystal orientation; mapping the sample orientation using DC-STEM complements the acquisition of HR images.

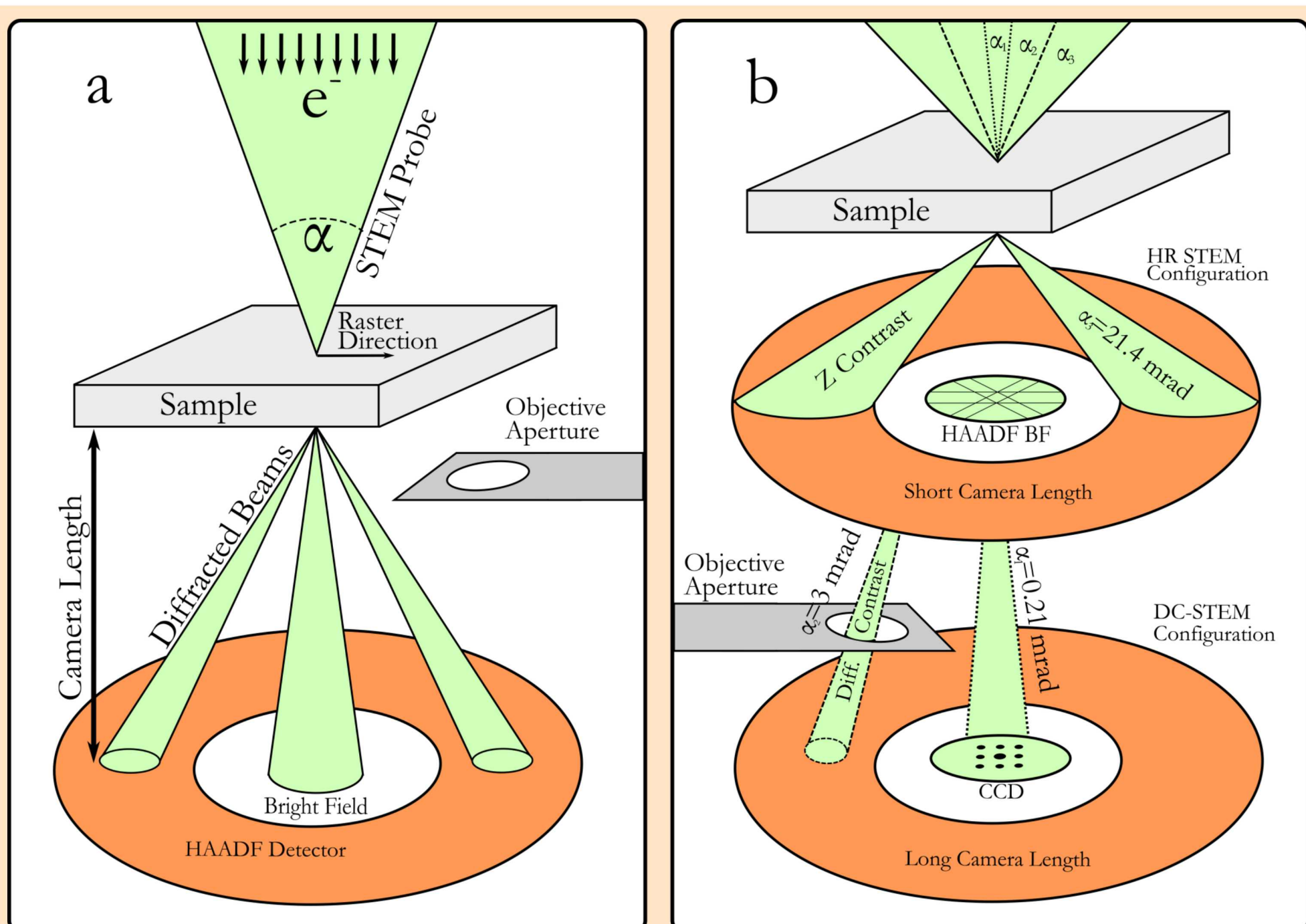


Figure 2: Schematics of the standard relationship between STEM probe, sample and types of information collected. a) shows the general relationship between important components required for imaging. b) Three microscope conditions used for data collection, changes in camera length are done electronically through lens current changes. DC-STEM is the only technique utilizing an objective aperture to select the imaging condition.

## Diffraction Pattern Identification

SingleCrystal<sup>TM</sup> diffraction pattern (DP) simulation software was used to confirm identification of experimentally acquired diffraction patterns.

- Measured lattice parameters for each phase are:  $a_{\gamma} = 3.47\text{ \AA}$ ,  $a_{\epsilon} = 2.448\text{ \AA}$ ,  $c_{\epsilon} = 4.08\text{ \AA}$ ,  $a_{\alpha} = 2.87\text{ \AA}$ ,  $c_{\alpha} = 2.96\text{ \AA}$ .
- Hydrogen charging does not affect the measured lattice constants of the observed  $\gamma$  or  $\epsilon$  phases.

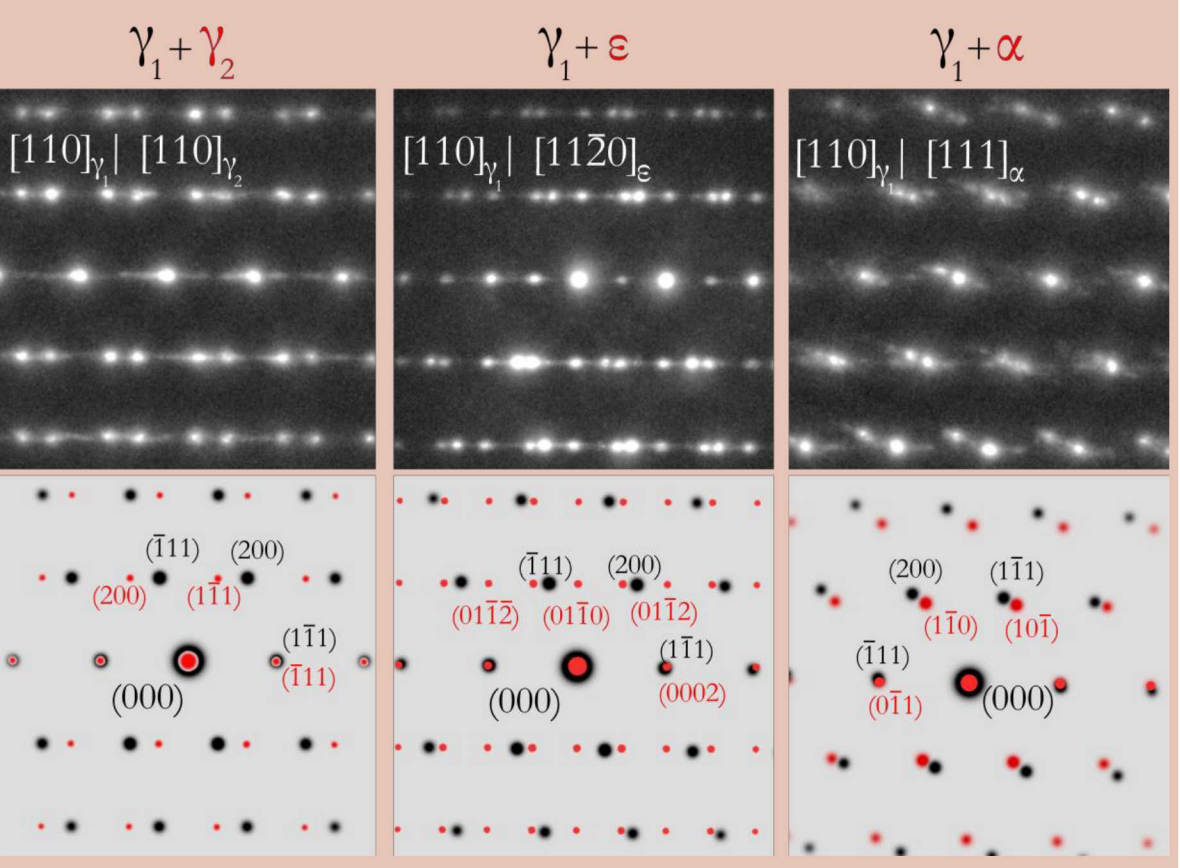


Figure 4: Nanodiffraction (Top) patterns and (bottom) simulations of phase boundaries within HC samples at 20% strain. Twins,  $\epsilon$ -, and  $\alpha$ -martensite have distinct relationships that relate close-packed planes. Twins and  $\epsilon$ -martensite show very clear overlay of DPs as the phase transitions are abrupt, completed through simple shear, while the FCC/BCC boundary pattern is smeared.

## Nucleation Mechanisms of Martensite

Multiple mechanisms describing the transformation of FCC austenite into BCC martensite have been proposed in the literature.<sup>[2,3,4]</sup>

- The passing of a single  $\frac{a}{6}\langle 112 \rangle$  partial dislocation produces a stacking fault(SF).
- Burgers and Bogers<sup>[2]</sup> have shown, through the use of a hard sphere model, that one third of the twinning shear ( $\frac{a}{6}\langle 112 \rangle\{111\}$  partial dislocation on every  $\{111\}$  plane) will produce the required configuration for a BCC lattice to form.
- The  $\frac{a}{18}\langle 112 \rangle$  twinning shear was proposed as a “spreading” of the dislocations, and is not experimentally verified.
- Olson and Cohen<sup>[3]</sup> later detailed the process by which  $\frac{a}{6}\langle 112 \rangle$  partial dislocation on alternate  $\{111\}$  produces a perfect HCP structure.
- Olson and Cohen described how two shears of one third and one half twinning shear can combine to form  $\alpha$ -martensite at the intersection of shear bands.<sup>[4]</sup>

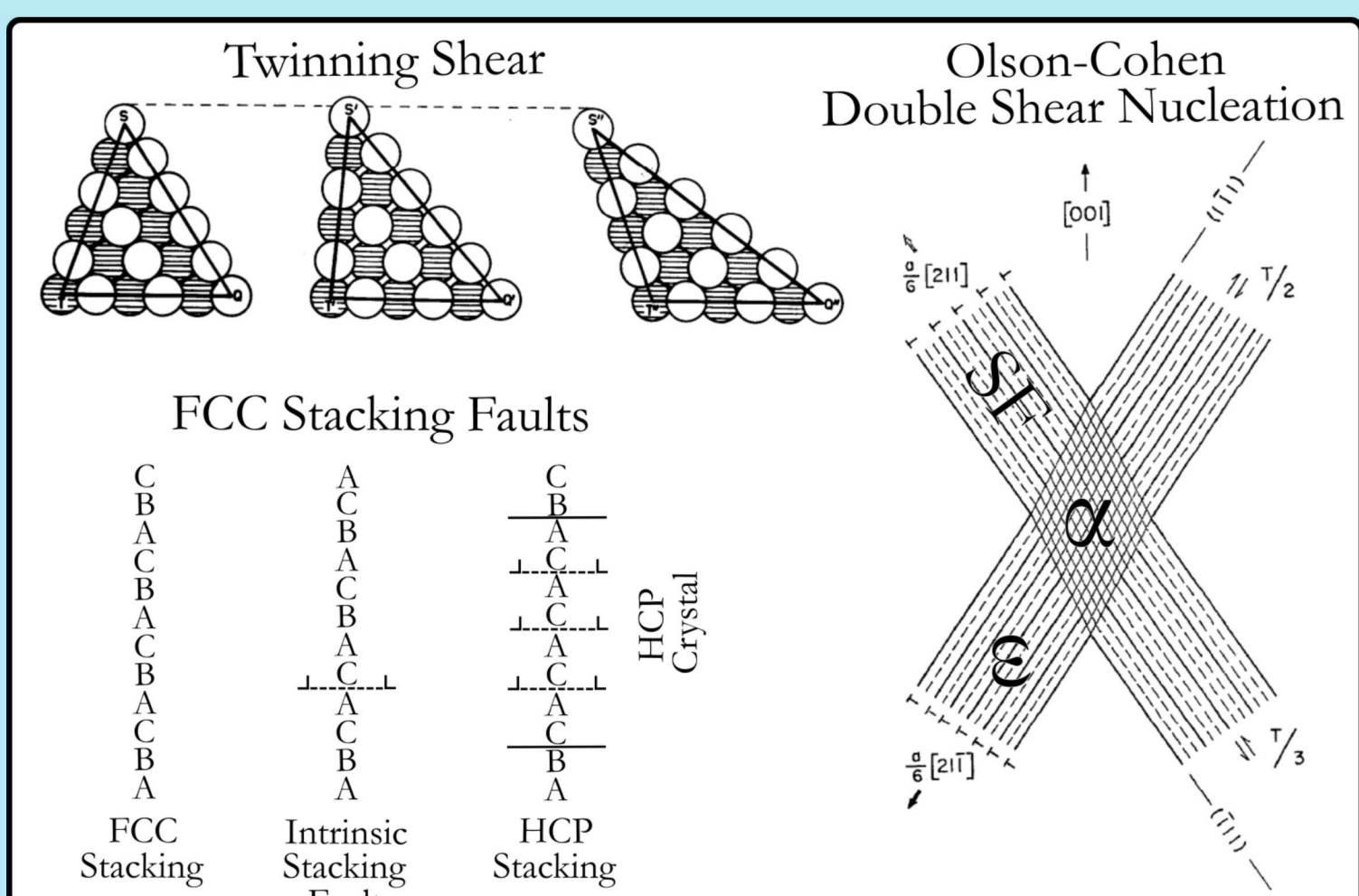


Figure 5: Example diagrams for the different mechanisms required in the formation of twins,  $\epsilon$ -, and  $\alpha$ -martensite. The twinning shear requires a  $\frac{a}{6}\langle 112 \rangle$  dislocation (a stacking fault) on every  $\{111\}$  to complete the twin shear (top left).<sup>[2]</sup> If the twin shear is only one third the total twinning shear, an BCC-like structure forms. Having a stacking fault on every other  $\{111\}$  plane produces ACAC stacking, or an HCP structure (bottom left).<sup>[3]</sup> Theoretically, two structures can intersect to produce a region of perfect BCC crystal, while allowing the partial  $\frac{a}{6}\langle 112 \rangle$  dislocations to continue propagating.<sup>[4]</sup>

## Conclusions

New insights into the effects of hydrogen on the formation of planar defects within 304L SS have been observed using advanced microscopy techniques.

- Changes in microstructure after straining in samples charged with hydrogen has been investigated using advanced STEM techniques.
- Dislocation activity appreciably decreases in HC SS, with strain being localized to planar defects, requiring the investigation of interface structure.
- In NC 20% strain samples, twinning is dominant over  $\epsilon$ -martensite formation with no  $\alpha$ -martensite observed down to a resolution of 3nm (NC results forthcoming in future work).
- $\epsilon$ -Martensite is a consistent intermediary in the formation of  $\alpha$ -martensite in HC SS, as seen with structures consistent with the “spreading” of  $\frac{a}{6}\langle 12\bar{1} \rangle_{\gamma}$  dislocations, the first observation of dislocation “spreading”.
- HR STEM imaging was successful in furthering the understanding of interfacial structures in martensite and the dislocation structures involved in martensite nucleation.